



ELSEVIER

Available online at www.sciencedirect.com

SCIENCE @ DIRECT®

Nuclear Instruments and Methods in Physics Research B xxx (2005) xxx–xxx

NIM B
 Beam Interactions
 with Materials & Atoms

www.elsevier.com/locate/nimb

Repulsive interatomic potentials for noble gas bombardment of Cu and Ni targets

M.A. Karolewski *

Department of Chemistry, University of Brunei Darussalam, Jalan Tungku Link, Gadong BE 1410, Brunei Darussalam, Borneo

Received 18 May 2005; received in revised form 3 July 2005

Abstract

Interatomic potentials that are relevant for noble gas bombardment of Cu and Ni targets have been calculated in the energy region below 10 keV. Potentials are calculated for the diatomic species: NeCu, ArCu, KrCu, Cu₂, ArNi, Ni₂ and NiCu. The calculations primarily employ density functional theory (with the B3LYP exchange–correlation functional). Potential curves derived from Hartree–Fock theory calculations are also discussed. Scalar relativistic effects have been included via the second-order Douglas–Kroll–Hess (DKH2) method. On the basis of a variational argument, it can be shown that the predicted potential curves represent an upper limit to the true potential curves. The potentials provide a basis for assessing corrections required to the ZBL and Molière screened Coulombic potentials, which are typically found to be too repulsive below 1–2 keV. These corrections significantly improve the accuracy of the sputter yield predicted by molecular dynamics for Ni(100), whereas the sputter yield predicted for Cu(100) is negligibly affected. The validity of the pair potential approximation in the repulsive region of the potential is tested by direct calculation of the potentials arising from the interaction of either an Ar or Cu atom with a Cu₃ cluster. The pairwise approximation represents the Ar–Cu₃ potential energy function with an error <3 eV at all Ar–Cu₃ separations. For Cu–Cu₃, the pairwise approximation underestimates the potential by ca. 10 eV when the interstitial atom is located near the centre of the cluster.

© 2005 Published by Elsevier B.V.

PACS: 31.15.Ew; 31.50.Bc; 79.20.Ap; 79.20.Rf

Keywords: Interatomic potentials; Molecular dynamics; Sputtering

1. Introduction

Molecular dynamics (MD) simulations provide a description of atomic collisions in solids within the framework of classical dynamics. In MD, atomic interactions are typically described by means of composite interatomic potentials. These consist of a repulsive screened Coulombic potential at short internuclear distances (R), which is interpolated to an attractive potential at internuclear distances that are shorter than chemical bond lengths.

For a pair of interacting atoms with atomic numbers Z_1 , Z_2 respectively, the repulsive potential may be expressed as

the product of the Coulombic potential and a screening function, $\phi(R)$, whose effect is to attenuate the internuclear repulsion

$$V(R) = (Z_1 Z_2 e^2 / 4\pi\epsilon_0 R) \phi(R). \quad (1)$$

For the most commonly used screened Coulombic potentials, the screening function is expressed as

$$\phi(R) = \sum_{k=1}^N c_k \exp(-b_k R/a). \quad (2)$$

For the Bohr potential, $N = 1$; for the Molière potential, $N = 3$; and for the Ziegler–Biersack–Littmark (ZBL) potential, $N = 4$ [1]. Standard values for the parameters c_k ,

* Tel.: +673 246 3001; fax: +673 246 1502.

E-mail addresses: mkarol@fos.ubd.edu.bn, karolewski@yahoo.com.

b_k are defined for each potential. The definition of the screening length a involves Z_1 and Z_2 , e.g. for the ZBL potential

$$a = 0.4685(Z_1^{0.23} + Z_2^{0.23})^{-1} (\text{\AA}). \quad (3)$$

Experimental determinations of repulsive interatomic potentials in condensed matter rely on fits to data obtained from scattering experiments. Low-energy ion scattering spectrometry (ISS) can be used to fit effective screening lengths up to several keV, but ISS data are mainly confined to light projectiles such as He^+ [2]. Schüller et al. made use of rainbow structures in the angular distributions of surface-channelled projectiles to test different functional forms of the repulsive projectile-target potential (up to ~ 40 eV) [3]. MD simulations of the Doppler broadening of gamma radiation produced during nuclear recoil de-excitation [4,5] or nuclear beta decay [6] can be used to evaluate potential functional forms in the approximate energy range 50–500 eV. For example, gamma ray induced Doppler shift data obtained for recoiling nuclei in Ni, Fe and Cr crystals have been used to fit the screening length for the ZBL potential [5]. ZBL screening length correction factors inferred in [5] were ca. 0.91 for the Fe–Fe and Ni–Ni potentials and ca. 0.78 for the Cr–Cr potential. Similarly, measured range parameters for heavy ions in amorphous solids can be compared with ranges simulated on the basis of an assumed potential function [7].

Repulsive interatomic potentials can be calculated via ab initio (first principles) quantum mechanical methods. For an isolated diatomic species (molecule or collision complex), the potential energy can be expressed in terms of the total electronic energy, $E_e(R)$ and the Coulombic internuclear repulsion, $U_n(R)$, as follows:

$$V(R) = U_n(R) + E_e(R) - E_e(\infty). \quad (4)$$

The final term in Eq. (4) arises because the potential energy is referenced to the energy of the separated atoms, i.e. $V(\infty) = 0$ by convention. Broomfield et al. calculated the ArCu^+ , ArSi and Si_2 potentials [8,9], while Kuwata et al. calculated potentials for ArCu and ArAl [10]. Other groups have calculated repulsive potentials for a range of homonuclear diatomics (predominately of light atoms) [11–14]. Errors on the order of 10% in the ZBL potential have been inferred from most of these studies.

In this paper, repulsive interatomic potentials have been calculated using ab initio methods for a number of heavy-atom diatomic species that are relevant for noble gas bombardment of Cu and Ni targets: NeCu , ArCu , KrCu , Cu_2 , ArNi , Ni_2 , NiCu . Sputter yield predictions for $\text{Cu}(100)$ and $\text{Ni}(100)$ targets from MD simulations based on the ZBL and the ab initio potentials respectively, are then compared.

Several sources of errors in calculated potentials can be identified, including basis set limitations and neglect of correlation and relativistic effects. Errors due to basis set lim-

itations are expected to increase at small internuclear separations [12]. There is no reliable database of potentials against which the accuracy of theoretical repulsive potentials can be tested. However, it will be shown in Section 4.1 that variational arguments can be used to identify regions in which an assumed analytic potential function is too repulsive. This method of evaluation provides a lower limit to the correction required for a particular form of analytic potential (e.g. the ZBL potential).

2. Computational methods

2.1. Interatomic potentials

Interatomic potentials were calculated using the Gaussian 03 suite of programs (revision B.05) [15]. A variety of theoretical methods and basis sets was employed. The calculations are primarily distinguished according to whether they employed the Hartree–Fock (HF) theory or the density functional theory (DFT). The hybrid B3LYP exchange–correlation functional was used for all of the DFT calculations reported here [16,17]. Both relativistic and non-relativistic HF and DFT calculations were carried out. Scalar (spin-independent) relativistic effects were taken into account using the second-order Douglas–Kroll–Hess (DKH2) method [18]. The relativistic calculations will be indicated in this paper using the notation HF–DKH2 and DFT–DKH2, while the unqualified designations of HF and DFT will be used for non-relativistic calculations.

The majority of calculations discussed in this paper employed the large all-electron basis set designated as 6-311 + G(3df), as implemented in Gaussian 03. This is a triple-zeta basis set (available for elements up to Kr) that is supplemented by polarization and diffuse functions. In Section 3.1 a number of calculations are reported that used the smaller all-electron 3-21 G and 6-31 G basis sets that lack polarization and diffuse functions. The Cu_2 DFT calculations from Gaussian were also compared with (non-relativistic) DFT calculations performed using the DMol3 quantum chemical package [19,20]. The DMol3 calculations used the hybrid BYLP exchange–correlation functional and the all-electron, double-numeric precision (DNP) basis set, which is comparable to the Gaussian 6-31 G(d) basis set.

Potential energy curves $V(R)$ for the diatomic species NeCu , ArCu , KrCu , Cu_2 and NiCu were calculated at 0.05 Å intervals of R for electronic states of the lowest spin multiplicity. For ArNi and Ni_2 , both singlet and triplet state potential energy curves were obtained. Calculations were performed for a range of R down to 0.3 Å, such that typically $V(R) < 5$ –8 keV. The potential energy scale is referenced either to the sum of free atom energies (the normal case, when the diatomic ground state dissociates into ground state atoms), or (for Cu_2 , Ni_2 and NiCu) to the diatomic energies at $R = 100$ Å.

2.2. Molecular dynamics

MD sputtering simulations were carried out using the Kalypso package (version 2.0) [21]. The projectile species was 3 keV Ar, incident from the normal direction. The Cu(100) and Ni(100) targets consisted of 13 atomic layers with 729 atoms per layer. Random Debye–Waller displacements were applied to target atoms, assuming a temperature of 300 K. The attractive parts of the Cu₂ and Ni₂ potentials were described using many-body tight-binding (TB) potentials smoothly cut off at 4.43 Å (Cu) and 4.32 Å (Ni) [22]. These potentials were interpolated to repulsive screened Coulombic potentials in the manner described in [21] in the regions 1.35–1.86 Å (Cu) and 1.05–1.85 Å (Ni). Purely repulsive potentials were used for ArCu and ArNi. Two types of repulsive potentials were used in the simulations: Bohr potentials fitted to the calculated DFT–DKH2 data, and uncorrected ZBL potentials (further details are given in Section 4.2). Electronic energy loss effects were taken into account by using the Lindhard–Scharff–Schjøtt (LSS) model [23]. Each simulation consisted of 325 projectile impact events directed into a zone of irreducible symmetry. Trajectories were followed for 10 ps. Atoms were considered to be sputtered if they were situated more than 10 Å above the surface layer at termination. Atoms that exit from the edge faces of the target (~5% of the sputter yield) are not included in the sputter yield estimates [24].

3. Results

3.1. Comparison of methods

A series of preliminary calculations of the Cu₂ potential was carried out in order to explore the sensitivity of the calculated potential energy curves to the choice of basis set. Fig. 1 compares potential energy curves for Cu₂ that were calculated with Gaussian and DMol3 using non-relativistic HF and DFT methods with a range of basis sets. The largest Gaussian basis set, 6-311 + G(3df), typically predicts the lowest potential energy at a given internuclear separation. Among the Gaussian calculations, the HF/3-21 G method, which involves the smallest basis set, gives rise to the highest potential energy. The potential energy curves calculated using the HF/3-21 G and HF/6-31 G methods lie above that calculated using the HF/6-311 + G(3df) method for $R < 0.85$ Å by 10–20%. There is good agreement between the potential curves calculated by the HF/6-311 + G(3df) and DFT/6-311 + G(3df) methods at the shorter internuclear distances (the mean deviation is 0.5% for $R < 1.1$ Å). The DMol3 DFT calculations predict a more repulsive potential for $R < 0.6$ Å than any of the Gaussian calculations, but for $R > 0.6$ Å the DMol3 predictions are comparable to those of the Gaussian HF/6-31 G method.

Fig. 2 compares Ar–Cu screening functions calculated using a variety of theoretical methods with the 6-

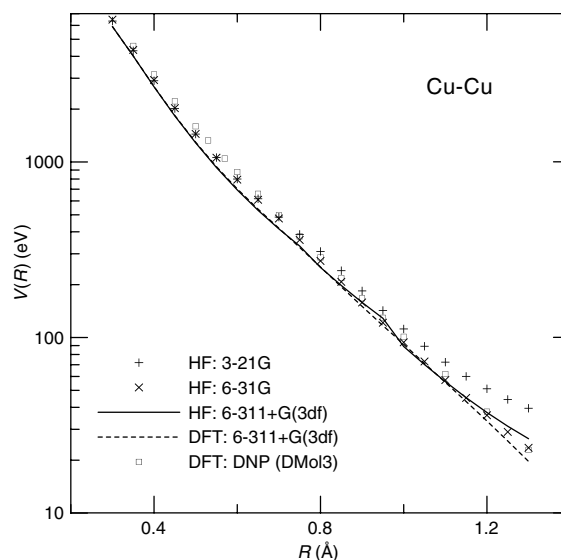


Fig. 1. Repulsive interatomic potentials for the Cu–Cu interaction calculated with non-relativistic Hartree–Fock (HF) and density functional theory (DFT) methods, and with various basis sets (see text).

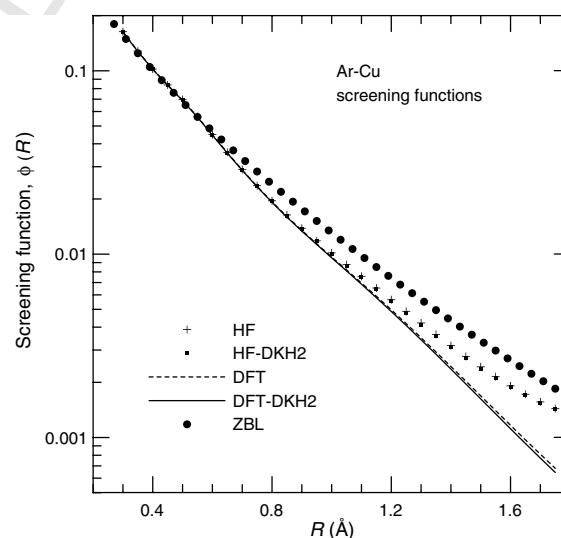


Fig. 2. Screening functions for the Ar–Cu interaction calculated with various theoretical methods. HF: Hartree–Fock theory; DFT: Density functional theory; HF–DKH2, DFT–DKH2: HF and DFT calculations that include second-order Douglas–Kroll–Hess scalar relativistic corrections. The ZBL potential is also illustrated.

311 + G(3df) basis set. The ZBL screening function is also shown for comparison. Relativistic and non-relativistic methods of calculation give rise to similar screening functions. The HF calculations predict screening functions that are somewhat more repulsive at large internuclear separations ($R > 1.2$ Å) than the screening functions predicted by the DFT calculations.

3.2. Diatomic potential energy curves

The ab initio potential energy curves presented in this section were obtained using the relativistic DFT–DKH2 method with the 6-311 + G(3df) basis set. All potential curve calculations were repeated using the HF–DKH2 method. The differences between relativistic and non-relativistic calculations were investigated in detail only for the Ar–Cu and Cu–Cu systems. Depending on whether correlation and (scalar) relativistic effects are included, different methods of calculation predict a considerable spread of total energies for the diatomic species. The following numerical results for the total energies of ArCu with $R = 1.0 \text{ \AA}$ and the 6-311 + G(3df) basis set are provided for illustration (expressed in hartrees, where $1 \text{ H} = 27.2114 \text{ eV}$): -2162.84145 (HF), -2165.35972 (DFT), -2176.66532 (HF–DKH2), -2179.19814 (DFT–DKH2). However, potential energy curves are derived from total energy differences. Good agreement between HF–DKH2 and DFT–DKH2 potential energy curves was obtained, except in the low energy region ($V < 30 \text{ eV}$). In this region, the DFT–DKH2 potential energy was typically found to be similar to, or lower than, the HF–DKH2 potential energy. The ArCu potential is not significantly influenced by relativistic effects, regardless of the calculation method (HF or DFT). For example, relativistic effects reduce the potential energy ($\sim 74 \text{ eV}$) predicted for ArCu at $R = 1.0 \text{ \AA}$ by 0.7 eV (HF) or by 0.8 eV (DFT) (cf. Fig. 2). However, relativistic effects lower the HF Cu_2 potential significantly (by $5\text{--}10 \text{ eV}$ even at large internuclear separations), but have little effect on the Cu_2 DFT potential.

The principal distinction between the HF and DFT methods of calculation is that the HF theory neglects the effects of electron correlation between electrons with opposing spins, while the latter includes it. Neglect of correlation in HF calculations leads to predictions of molecular dissociation energies that may be in error by 10 eV or more for transition metal systems. Although the HF theory cannot be used reliably for thermochemical calculations that involve transition metals, a discrepancy of this magnitude is acceptable in calculations of repulsive potential energy curves in the more repulsive region of the potential.

Figs. 3–5 display DFT–DKH2 potential energy curves computed for the following systems: NeCu, KrCu, ArNi, ArCu, Cu_2 , Ni_2 . Table 1 presents a summary of the calculations in numerical form, and also includes data for the NiCu potential function that is not shown in the figures. For Ni_2 and ArNi, ab initio potential energy curves are presented for both the singlet and triplet molecular states. Multiplicity effects in Ni_2 and ArNi produce modifications of the potential that become significant at large internuclear separations ($r > 1.2 \text{ \AA}$). Figs. 3–5 also compare the ab initio potential functions with the ZBL and Molière potential functions. The ZBL potential data are unadjusted. The Molière potential data have been computed using the Lindhard screening length formula, and following common

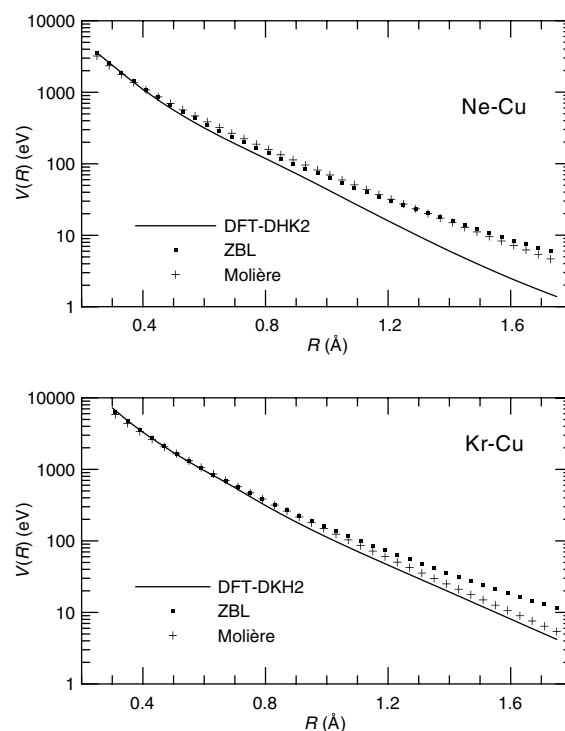


Fig. 3. Comparison of calculated (DFT–DKH2) interatomic potential functions for NeCu (top) and KrCu (bottom) with the corresponding ZBL and Molière potentials.

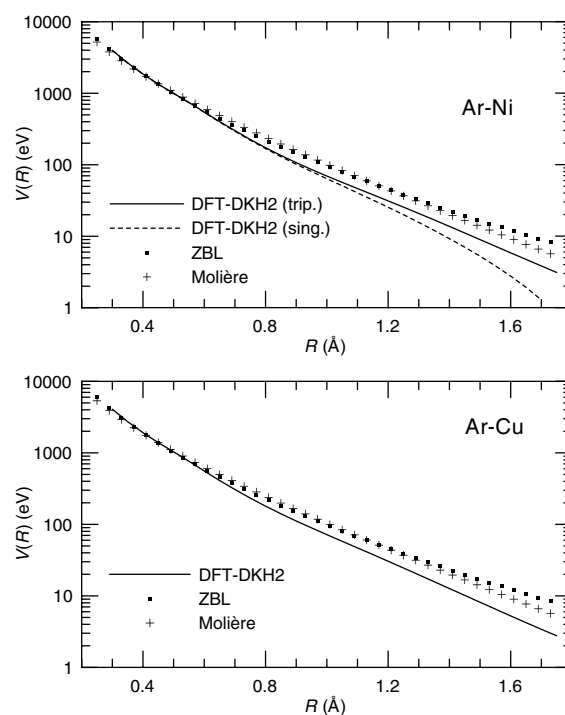


Fig. 4. Comparison of calculated (DFT–DKH2) interatomic potential functions for ArNi (top) and ArCu (bottom) with the corresponding ZBL and Molière potentials.

practice in the ion scattering community, this screening length has been adjusted by a factor of 0.8; this adjustment

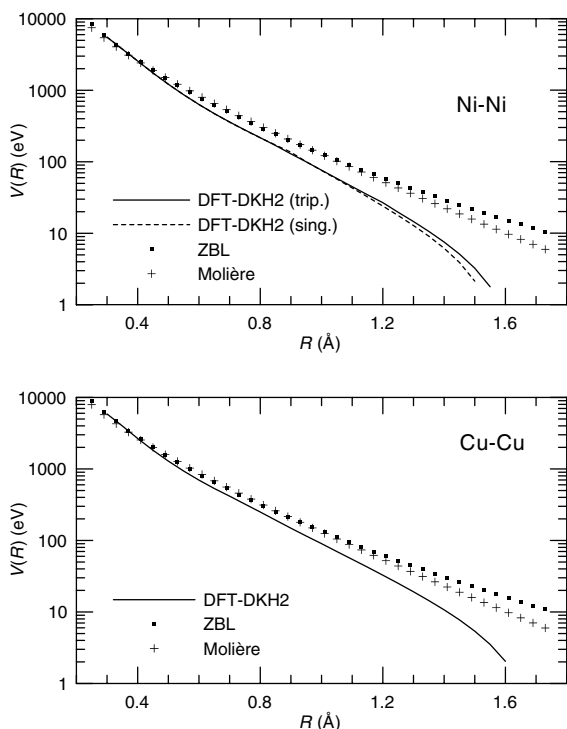


Fig. 5. Comparison of calculated (DFT-DKH2) interatomic potential functions for Ni_2 (top) and Cu_2 (bottom) with the corresponding ZBL and Molière potentials.

arise for diatomic species that exhibit chemical interactions (Ni_2, Cu_2). The negative curvature of the potential function in the region that precedes the attractive potential well cannot be represented using a screening function based on positive exponential terms. Thus, divergence of any potential with the mathematical form of Eq. (2) from the downward-turning part of the ab initio potential is inevitable as R increases. For large internuclear separations the Molière potential gives slightly better agreement with the ab initio data for most systems than does the ZBL potential.

3.3. Atom-cluster potential energy curves

In practical applications of interatomic potentials (e.g. MD) the repulsive part of the diatomic potential is generally assumed to be transferable to the solid state environment. In order to test the validity of this assumption, potential functions were computed for the approach of an ‘interstitial’ atom X (where $X = \text{Cu}$ or Ar) towards one vertex of a rigid D_{3h} Cu_3 cluster, using the DFT-DKH2 method (this cluster is a structural unit of $\text{Cu}(111)$ planes). The geometry of the arrangement is shown in Fig. 6. In Table 2, the 4-atom potential energy calculations are compared with potential energies that are computed using a summation of terms from the corresponding diatomic ($X\text{--Cu}$) pair potentials (Figs. 4 and 5). Table 2 indicates that the pair potential sum produces a good representation of the Ar--Cu_3 potential energy function, even at large Ar--Cu separations (error < 3 eV). However, for the Cu--Cu_3 system, the pair potential sum underestimates the potential by as much as 10 eV. This happens because the mean cluster binding energy becomes less attractive as the coordination number increases. Thus, using the $\text{Cu} + \text{Cu}_3$ asymptote as the potential zero, the

Table 1

Ab initio diatomic potential energy functions $V(R)$ calculated using the DFT-DKH2 method

R (Å)	$V(R)$ (eV)						
	Ne–Cu	Ar–Cu	Kr–Cu	Cu–Cu	Ar–Ni	Ni–Ni	Ni–Cu
0.30	2395.4	4071.2	7249.0	5880.8	3977.1	5538.0	5702.8
0.35	1604.1	2734.5	4785.5	3991.2	2663.7	3766.1	3885.9
0.40	1100.4	1913.5	3305.9	2668.1	1853.6	2566.0	2616.5
0.45	776.8	1391.3	2364.6	1825.2	1339.0	1744.4	1783.9
0.50	563.5	1034.4	1717.6	1285.8	994.8	1213.3	1248.6
0.55	418.5	762.4	1272.5	933.1	738.4	864.8	898.2
0.60	317.3	558.1	962.8	696.8	540.4	631.5	663.6
0.65	244.6	411.4	737.5	533.7	396.5	471.6	502.2
0.70	191.0	307.6	555.7	416.1	294.1	358.9	387.8
0.75	150.3	233.5	415.3	322.8	221.0	277.1	303.0
0.80	118.7	180.0	312.8	249.9	168.5	216.3	236.3
0.90	72.9	112.4	183.6	148.7	101.8	135.9	141.6
1.00	44.0	71.8	112.6	90.3	63.8	75.8	84.2
1.10	26.4	46.8	71.2	54.4	40.5	43.1	50.6
1.20	15.9	30.5	45.9	32.7	25.4	24.0	30.7
1.30	9.7	19.7	29.8	19.1	15.6	12.8	18.3
1.40	6.0	12.7	19.3	10.7	9.3	6.2	10.6
1.50	3.8	8.1	12.5	5.4	5.3	2.1	5.8

Data refer to the diatomic state of the lowest spin multiplicity. The calculated potentials represent upper estimates to the true potentials (see text).

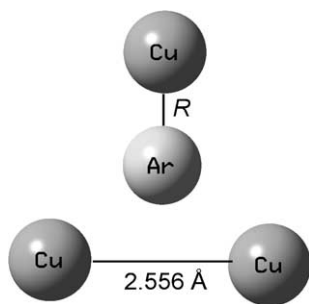


Fig. 6. Structure used for calculation of the 4-body Ar-Cu₃ cluster potential, $V(R)$. The Cu atom positions remain fixed as the internuclear separation parameter, R , is varied. A similar structure, with replacement of Ar by Cu, was used for the Cu-Cu₃ calculations. The zero level of the potential energy scale corresponds to the limit $R \rightarrow \infty$.

Table 2

Ab initio 4-atom (X-Cu₃) potential energies for the approach of an atom X (where X = Cu or Ar) towards one vertex of a D_{3h} Cu₃ cluster (see Fig. 6 for definition of the internuclear separation, R)

R (Å)	X = Cu		X = Ar	
	4-Atom (eV)	Pair (eV)	4-Atom (eV)	Pair (eV)
0.50	1290.2	1280.7	1037.7	1036.2
0.70	415.2	411.1	310.6	309.9
0.80	250.9	245.9	184.0	183.4
0.90	151.1	145.4	116.9	116.1
1.00	94.0	88.4	78.8	77.1
1.48	28.6	19.6	30.2	27.4

The 4-atom potential energy calculations are compared with potential energies based on a summation of terms from the corresponding ab initio diatomic (X-Cu) pair potentials.

$$V_C(R) = U_n(R) + E_e(R) + \Delta E_e(R) - E_e(\infty) - \Delta E_e(\infty) = V(R) + \Delta V(R), \quad (5)$$

where the error term $\Delta V(R)$ represents the difference of the error terms ΔE_e associated with the diatomic and separated configurations of the interacting atoms:

$$\Delta V(R) = \Delta E_e(R) - \Delta E_e(\infty). \quad (6)$$

The origin and significance of these error terms will depend on the type of calculations involved. For example, a non-relativistic Hartree-Fock calculation might include errors due to basis set limitations, and to neglect of correlation and relativistic effects. The sign of ΔV will then be determined by the extent to which these errors change during molecule formation. Errors due to neglect of correlation might be expected to show up in comparisons between Hartree-Fock calculations (which neglect correlation) and DFT calculations (which include it). Figs. 1 and 2 demonstrate agreement between the HF and DFT potentials, except in the low energy tails of the potentials, and support the conclusion reached by Nordlund et al. that the accuracy of repulsive potentials is determined by basis set limitations rather than by the level of theory [12]. For the diatomic species and internuclear separations considered here, relativistic scalar effects appear to be unimportant in determining the repulsive potential because they largely cancel out when energy differences are obtained (Fig. 2). Non-scalar relativistic effects (i.e. spin-orbit interactions), which are neglected in the Gaussian implementation of the DKH2 method, could conceivably affect the potentials, but without further specialised calculations it is difficult to assess their importance.

Basis set exponents and expansion coefficients are normally optimised so as to minimize the energy of the atomic ground state at a certain level of theory. For example, the 6-311 + G(3df) basis set minimizes the energy of the atomic ground state at the MP2 (second-order Møller-Plesset) perturbation level, i.e. $\Delta E_e(\infty)$. It is reasonable to assume that any deficiency (error) in the calculation of electronic energies due to basis set limitations will worsen (or stay the same) in the repulsive region of the molecular potential. Therefore in situations where basis set error is the dominating contribution to ΔV (i.e. when R is much smaller than the equilibrium internuclear distance), this assumption is equivalent to the assertion that $\Delta E_e(R) \geq \Delta E_e(\infty)$, or $\Delta V(R) \geq 0$ (Eq. (6)). It follows from Eq. (5) that under these conditions the predicted potential energy $V_C(R)$ overestimates $V(R)$, so that $V_C(R)$ represents an upper limit to the true potential energy. This relationship explains why potential curves calculated with the 3-21 G and 6-31 G basis sets (Fig. 1) give rise to potential energy curves that lie above the curve calculated using the larger 6-311+G(3df) basis set: as the basis set flexibility improves, the potential energy curves become more accurate.

The interpretation of the ab initio potential energy curve as an upper limit to the true potential energy curve finds a practical application in situations where the ab initio po-

binding energy of the interstitial to the 3-atom cluster is reduced relative to the pairwise sum of diatomic binding energies, which corresponds to a higher potential. The largest error in the pairwise approximation arises near $R = 1.5$ Å, when the interstitial atom is at the centre of the cluster. The difficulty of modelling this region of the potential in MD simulations has long been recognised [25]. The effects of coordination number can be handled in principle using many-body potentials, but if the latter are fitted to properties near the equilibrium bond distance (the usual case) they may not produce correct behaviour in the repulsive region.

4. Discussion

4.1. Significance of potential energy curves

Quantum chemical codes rely on variational methods (in practice DFT and DKH2 methods are only approximately variational), which provide an upper limit, $E_e(R) + \Delta E_e(R)$, to the exact electronic energy of the molecular ground state. The direction of the energy error, $\Delta E_e(R)$, is known, but not its magnitude. The internuclear repulsion, $U_n(R)$, can be calculated precisely. Thus, using Eq. (4), a calculated (C) potential, $V_C(R)$, stands in the following relation to the true potential $V(R)$:

tential is lower than an analytical potential. Figs. 3–5 show that this is generally the case for the Molière and ZBL potentials in the energy regime below 1–2 keV that is important for sputtering simulations. Thus, it becomes possible to indicate the direction in which each potential should be corrected, and to specify the minimum required correction.

4.2. Application to sputtering

The accuracy required of a repulsive interatomic potential depends upon the intended application. High-yield sputtering events are initiated by close encounters between projectile and target atoms [26]. The maximum attainable value for the projectile-target potential energy is equal to the centre of mass (COM) energy of a direct impact collision, V_{MAX} [27]

$$V_{\text{MAX}} = m_2/(m_1 + m_2)E_p, \quad (7)$$

where E_p is the incident projectile energy, and m_1 and m_2 are the masses of the projectile and target atoms respectively. The maximum attainable value of the potential energy in a collision between a recoiling target atom (created by the same projectile) can similarly be calculated from standard energy-transfer formulae [1].

For example, the simulation of Cu sputtering by 3 keV Ar projectiles will require an ArCu potential that is defined up to 1842 eV and a Cu₂ potential that is defined up to 1422 eV. Fig. 4 shows that the ZBL and Molière ArCu potentials are in good agreement with the ab initio ArCu potential from 1842 eV (i.e. V_{MAX}) down to about 900 eV, then deviate to more positive values. From the discussion given in Section 4.1 it can be concluded that the ZBL and Molière ArCu potentials are too repulsive in the region where $V(R) < 900$ eV (i.e. $R > 0.52$ Å). Likewise, Fig. 5 shows that the ZBL and Molière Cu₂ potentials are more repulsive than the ab initio Cu₂ potential in the entire region where $V(R) < 1422$ eV. In the regions where the ZBL or Molière potentials are more repulsive than the ab initio potentials, they require correction, in the form of a downward adjustment, that at a minimum will bring them into coincidence with the ab initio potentials.

In order to test the ab initio potential data in sputtering simulations, Bohr potentials (Eq. (2)) were fitted to the ab initio DFT–DKH2 ArCu, ArNi, Cu₂ and Ni₂ potentials in the energy regions of interest for 3 keV Ar sputtering of Cu and Ni targets. The fitting parameters are collected in Table 3. The fitting procedure involved least squares minimisation of the fractional (not absolute) deviation terms. Fig. 7 shows the composite potentials that were constructed for use in the simulations by interpolating the repulsive Ni₂ and Cu₂ potentials to tight-binding potentials (Section 2.2). The fitted Bohr potentials give better representations of the ab initio potentials than do the uncorrected ZBL and Molière potentials. Addition of further exponential terms to the screening function did not significantly improve any of the fits.

Table 3

Parameters and fitting ranges of R for the Bohr potential screening function $\phi(R) = A\exp(-bR)$ derived from fits to the ab initio (DFT–DKH2) potential curves for ArNi, ArCu, Ni₂ and Cu₂, where R is the internuclear separation

	A	b (Å ⁻¹)	R (Å)
Ar–Ni	0.54503	4.1735	0.405–1.500
Ar–Cu	0.53120	4.1174	0.405–1.500
Ni–Ni	0.45531	4.2980	0.475–1.200
Cu–Cu	0.37399	3.9357	0.485–1.200

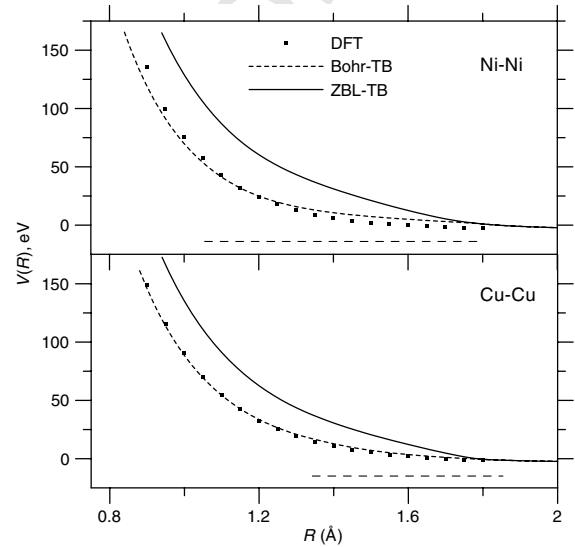


Fig. 7. Comparison of Bohr–TB and ZBL–TB composite potentials for Ni₂ (top) and Cu₂ (bottom). The calculated (DFT–DKH2) interatomic potential functions for the same species are also shown. The horizontal dashed lines indicate the lengths of the interpolation regions for the composite potentials.

The energy regions of the potential energy curves that lie below the sputtering threshold energy (about 10–20 eV) do not affect the sputtering predictions, but may affect predictions of other types of radiation damage. For example, interstitial defect atoms in Cu and Ni have neighbours at 1.5–1.8 Å, while projectiles with energies below the sputtering threshold may still be capable of producing adatoms and vacancies. Typically, the same region is used for interpolation of the repulsive and attractive potentials. Kalypso employs a linear combination of the repulsive and attractive potentials, using weights that depend on R [21]. The properties of the potential in the interpolation region thus vary continuously between those of the repulsive and attractive potentials.

Sputter yields predicted by the MD simulation method described in Section 2.2 for Cu(100) and Ni(100) under 3 keV Ar projectile bombardment are compared with experimental estimates [28,29] in Table 4. The simulations differ in terms of the potentials used in the repulsive regions, i.e. either the uncorrected ZBL potential or the Bohr potential with parameters fitted to ab initio (DFT–DKH2) data. The predicted sputter yields for Cu(100) were found

Table 4

Comparison of sputter yields predicted for Cu(100) and Ni(100) targets by simulations that employ either Bohr potentials fitted to DFT–DKH2 data, or ZBL potentials, to model repulsive interactions

System	Bohr	ZBL	Exp.
3 keV Ar → Cu(100)	4.7 ± 0.3	4.6 ± 0.3	4.0 [28]
3 keV Ar → Ni(100)	3.6 ± 0.3	4.2 ± 0.2	2.2 ^a

Experimental values (Exp.) are also listed. Quoted uncertainties represent the standard error.

^a Estimated from value for polycrystalline (polyx) Ni [29] and polyx/(100) ratio for Cu [28].

when the interstitial atom is located near the centre of the cluster.

Acknowledgements

Financial support from the University of Brunei Darussalam is gratefully acknowledged.

References

- [1] W. Eckstein, Computer Simulation of Ion–Solid Interactions, Springer, New York, 1991.
- [2] Th. Fauster, D. Hartwig, H. Dürr, Appl. Phys. A 45 (1988) 63.
- [3] A. Schüller, S. Wethekam, A. Mertens, K. Maass, H. Winter, K. Gärtner, Nucl. Instr. and Meth. B 230 (2005) 172.
- [4] J. Keinonen, A. Kuronen, P. Tikkanen, H.G. Börner, J. Jolie, S. Ulbig, E.G. Kessler, R.M. Nieminen, M.J. Puska, A.P. Seitsonen, Phys. Rev. Lett. 67 (1991) 3692.
- [5] N. Stritt, J. Jolie, M. Jentschel, H.G. Börner, C. Doll, J. Res. Natl. Inst. Stand. Technol. 105 (2000) 71.
- [6] V. Vorobel, C. Briancon, V. Brudanin, V. Egorov, J. Deutsch, R. Prieels, N. Severijns, Y. Shitov, C. Vieu, T. Vlyov, I. Yutlandov, S. Zaparov, Eur. Phys. J. A 16 (2003) 139.
- [7] E. Friedland, S. Kalbitzer, M. Hayes, C. Klatt, G. Komac, C. Langpape, Nucl. Instr. and Meth. B 136–138 (1998) 147.
- [8] K. Broomfield, R.A. Stansfield, D.C. Clary, Surf. Sci. 202 (1988) 320.
- [9] K. Broomfield, R.A. Stansfield, D.C. Clary, Phys. Rev. B 39 (1989) 7680.
- [10] K. Kuwata, R.I. Erickson, J.R. Doyle, Nucl. Instr. and Meth. B 201 (2003) 566.
- [11] J.M. Pruneda, E. Artacho, Phys. Rev. B 70 (2004) 035106.
- [12] K. Nordlund, N. Runeberg, S. Sundholm, Nucl. Instr. and Meth. B 132 (1997) 45.
- [13] J. Keinonen, A. Kuronen, K. Nordlund, R.M. Nieminen, A.P. Seitsonen, Nucl. Instr. and Meth. B 88 (1994) 382.
- [14] H.Y. Chan, K. Nordlund, J. Peltola, H.J. Gossmann, N.L. Ma, M.P. Srinivasan, F. Benistant, L. Chan, Nucl. Instr. and Meth. B 228 (2004) 240.
- [15] Gaussian, Inc., Pittsburgh PA.
- [16] A.D. Becke, J. Chem. Phys. 98 (1993) 5648.
- [17] C. Lee, W. Yang, R.G. Parr, Phys. Rev. B 37 (1988) 785.
- [18] M. Barysz, A.J. Sadlej, Theochem 573 (2001) 181.
- [19] B. Delley, J. Chem. Phys. 92 (1990) 508.
- [20] B. Delley, J. Chem. Phys. 113 (2000) 7756.
- [21] M.A. Karolewski, Nucl. Instr. and Meth. B 230 (2005) 402.
- [22] F. Cleri, V. Rosato, Phys. Rev. B 48 (1993) 22.
- [23] J. Lindhard, M. Scharff, H.E. Schiøtt, K. Dan, Vidensk. Selsk. Mat. Fys. Medd. 33 (1966) 14.
- [24] M.A. Karolewski, Nucl. Instr. and Meth. B 211 (2003) 43.
- [25] H.M. Urbassek, Nucl. Instr. and Meth. B 122 (1997) 427.
- [26] M.H. Shapiro, P. Lu, Nucl. Instr. and Meth. B 215 (2004) 326.
- [27] M. Gryziński, Phys. Rev. 138 (1965) A305.
- [28] H.E. Roosendahl, in: R. Behrisch (Ed.), Sputtering by Particle Bombardment I, Springer, Berlin, 1981, p. 219.
- [29] Y. Yamamura, H. Tawara, At. Data Nucl. Data Tables 62 (1996) 149.

to be similar, within statistical uncertainties, for the ZBL and Bohr potentials. The sputter yields predicted for Ni(100) using the Bohr potentials were about 14% lower than those predicted using the ZBL potentials, which is statistically significant, and reduces the discrepancy with experiment. The ArNi and ArCu potential corrections are quite similar in absolute and fractional terms. The reduction in sputter yield predicted for Ni(100) mainly arises because the ZBL potential overstates the nuclear stopping of Ni in Ni (the corrections required for the Ni₂ ZBL potential are larger than those required for the Cu₂ ZBL potential, as indicated in Fig. 6). For example, at $R = 1.05 \text{ \AA}$ the ZBL Ni–Ni potential (106 eV) is some 85% higher than the Bohr Ni₂ potential (57 eV), whereas the Cu₂ ZBL potential (111 eV) is only 58% higher than the Bohr Cu–Cu potential (70 eV).

5. Conclusions

Interatomic potentials have been calculated for the following diatomic species in the energy region below 10 keV: NeCu, ArCu, KrCu, Cu₂, ArNi, Ni₂ and NiCu. On the basis of a variational argument, it can be shown that the predicted potential curves represent an upper limit to the true potential curves. The predicted potentials provide a basis for assessing corrections required to the ZBL and Molière screened Coulombic potentials, which are typically found to be too repulsive below 1–2 keV. These corrections significantly improve the accuracy of the sputter yield predicted by MD simulations for Ni(100), but the sputter yield predicted for Cu(100) is negligibly affected. The validity of the pair potential approximation in the repulsive region of the potential is tested by direct calculation of the potentials arising from the interaction of either an Ar or Cu atom with a Cu₃ cluster. The pairwise approximation provides a fairly good representation of the Ar–Cu₃ potential energy function (<3 eV error), at all Ar–Cu₃ separations. For the Cu–Cu₃ system, the pairwise approximation underestimates the potential by ca. 10 eV